HHS Public Access

Author manuscript

Neuron. Author manuscript; available in PMC 2022 December 01.

Published in final edited form as:

Neuron. 2021 December 01; 109(23): 3851–3861.e4. doi:10.1016/j.neuron.2021.09.021.

Sleep replay reveals premotor circuit structure for a skilled behavior

Margot Elmaleh[1,2], **Devorah Kranz**[1,2], **Ariadna Corredera Asensio**[1,2], **Felix W. Moll**[1,2], **Michael A. Long**[1,2,3,*]

[1]NYU Neuroscience Institute and Department of Otolaryngology, New York University Langone Medical Center, New York, NY 10016 USA

[2]Center for Neural Science, New York University, New York, NY, 10003 USA

SUMMARY

Neural circuits often exhibit sequences of activity, but the contribution of local networks to their generation remains unclear. In the zebra finch, song-related premotor sequences within HVC may result from some combination of local connectivity and long-range thalamic inputs from nucleus uvaeformis (Uva). Because lesions to either structure abolish song, we examine 'sleep replay' using high-density recording methods to reconstruct precise song-related events. Replay activity persists after the upstream nucleus interfacialis of the nidopallium is lesioned and slows when HVC is cooled, demonstrating that HVC provides temporal structure for these events. To further gauge the importance of intra-HVC connectivity for shaping network dynamics, we lesion Uva during sleep and find that residual replay sequences can span syllable boundaries, supporting a model in which HVC can propagate sequences throughout the duration of the song. Our results highlight the power of studying offline activity for studying behaviorally relevant circuit organization.

Graphical Abstract

[*]To whom correspondence should be addressed: Michael A. Long (mlong@med.nyu.edu).

[3]Lead contact

Author contributions: M.E. and M.A.L conceived the study and designed the experiments; M.E., F.W.M., A.C.A., and D.K. conducted the research; M.E. and M.A.L. performed data analyses; M.E. and M.A.L. created the figures; M.E. wrote the initial draft of the manuscript; M.E., F.W.M., and M.A.L. edited and reviewed the final manuscript; M.E. and M.A.L. acquired funding; M.A.L. supervised the project.

Declaration of interests: The authors declare no competing interests.

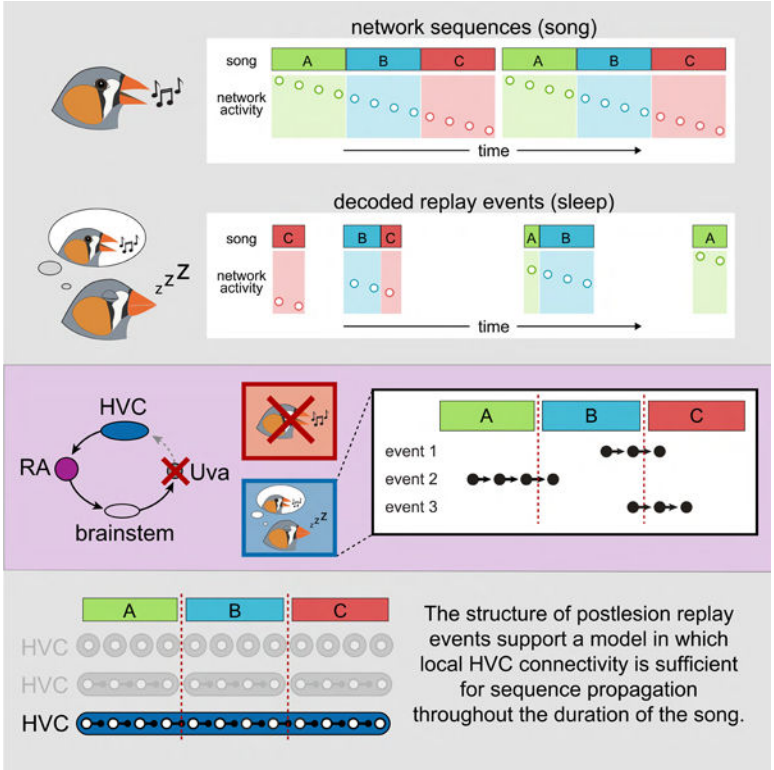

eTOC:

Elmaleh et al. use high density recordings to measure the activity of the song control pathway in the zebra finch. They precisely decode snippets of song-related activity during sleep and leverage these ‘offline’ dynamics to test three models of network connectivity responsible for sequence generation.

Keywords

birdsong; sequences; network; vocal production; zebra finch; motor control; circuit models

INTRODUCTION

Neuronal sequences have been proposed to perform important functions in many brain regions, such as navigation (Skaggs et al., 1996), time generation (MacDonald et al., 2011; Pastalkova et al., 2008), decision making (Harvey et al., 2012; Schmitt et al., 2017), and skilled movement (Peters et al., 2014). The zebra finch has emerged as an excellent model system for studying the mechanisms underlying neural sequences that drive a well-defined complex behavior (Hahnloser et al., 2002). Through months of intensive practice (Tchernichovski et al., 2001), male zebra finches learn to produce a highly stereotyped courtship song, consisting of a repeated series of 2–7 distinct vocal elements called syllables. During singing, a sparse sequence of activity is generated within the forebrain nucleus HVC (proper name) in which each premotor neuron produces a single high-frequency burst of spikes (duration: ~10ms) (Hahnloser et al., 2002; Kozhevnikov and

Fee, 2007); as a population, these neurons form a temporally precise (jitter with respect to song: < 1 ms) neural sequence tiling the length of the song (Egger et al., 2020; Lynch et al., 2016; Picardo et al., 2016) (Figure 1A). HVC activity is then sent to the robust nucleus of the arcopallium (RA) and ultimately to motor neurons and song-production musculature (Wild, 1993) (Figure 1B).

Previous electrophysiological (Kosche et al., 2015; Mooney and Prather, 2005) and ultrastructural (Kornfeld et al., 2017) work has demonstrated that premotor HVC neurons form synapses with each other, and these local axon collaterals have been proposed to act as a means of propagating activity by sequentially activating premotor neurons during song (Egger et al., 2020; Fee et al., 2004; Long et al., 2010). In addition, local circuit GABAergic interneurons (Scotto-Lomassese et al., 2007; Wild et al., 2005) provide inhibition that may also contribute to premotor patterning (Gibb et al., 2009; Kosche et al., 2015; Markowitz et al., 2015).

Along with this intrinsic circuitry, HVC receives input from a multi-region feedback loop dedicated to song production. Feedback signals must pass through the vocal thalamic nucleus uvaeformis (Uva) that projects both directly to HVC and indirectly via a cortical sensorimotor region known as the nucleus interfacialis of the nidopallium (NIf) (Figure 1B) (Coleman and Mooney, 2004; Hahnloser and Fee, 2007; Hahnloser et al., 2008; Reinke and Wild, 1998; Striedter and Vu, 1998). Together, NIf and Uva provide the two main sources of external input to HVC. While NIf has been demonstrated to be important for song learning in juvenile birds (Mackevicius et al., 2020; Roberts et al., 2012; Zhao et al., 2019), it does not play a critical role in adult song production; complete lesions of NIf only temporarily perturb singing (Cardin et al., 2005; Otchy et al., 2015). In contrast, lesions to either HVC or Uva can permanently abolish song production (Coleman and Vu, 2005; Danish et al., 2017; Nottebohm et al., 1976; Williams and Vicario, 1993). A clear understanding of how local connectivity and external inputs (e.g., from Uva) work together to enable sequence generation and propagation in HVC remains elusive (Andalman et al., 2011; Galvis et al., 2017; Hamaguchi et al., 2016; Long et al., 2010). A similar barrier also exists in many other systems, where elimination of either cortical or thalamic activity disrupts both behavior and circuit dynamics in the intact region (Bolkan et al., 2017; Guo et al., 2017; Sauerbrei et al., 2020; Schmitt et al., 2017).

There are three existing classes of models for how local circuitry and long-range inputs contribute to the premotor sequence observed during song, with the key difference being the timescale represented within the HVC microcircuit. In the *distributed model* (Figure 1C), sequence progression is critically reliant upon moment-to-moment feedback through Uva (Hamaguchi et al., 2016). Here, local HVC circuitry is not sufficient to advance the sequence; thus, the relevant timescale produced within HVC is limited to the duration of a premotor burst (**~ 10 ms**). The remaining models rely on intrinsic HVC connections to propagate sequential activity (Figures 1D and 1E). In the *subnetwork model* (Figure 1D), HVC is composed of multiple discrete subcircuits that encode individual song elements (**~ 100–200 ms**) (Glaze and Troyer, 2006; Long and Fee, 2008; Wang et al., 2008). In this view, HVC lacks the local connectivity to link the subnetworks, a role performed by extrinsic influences, likely from the feedback loop (Andalman et al., 2011). A subnetwork

organization based on syllables is consistent with previous behavioral perturbations that abolish singing at syllable boundaries rather than at arbitrary moments during the song (Cynx, 1990; Galvis et al., 2017). In contrast, the HVC microcircuit may have sufficient information in its intrinsic connections to form a single continuous network sequence (**~ 1 s**) representing a concatenation of each song element within the finch's repertoire (*continuous model*, Figure 1E).

To address these models, we first performed high-density recordings within the zebra finch song control pathway during song performance. We found that Uva lesions not only abolished singing (Coleman and Vu, 2005; Danish et al., 2017; Williams and Vicario, 1993) but also eliminated all song-related activity, preventing our ability to study HVC circuit structure. We therefore turned our attention to previously observed 'replay' events occurring during sleep (Dave and Margoliash, 2000; Hahnloser et al., 2006; Long et al., 2010) as a means of testing models of HVC circuit organization outside of the context of singing. We decoded the activity of neural ensembles within the song control pathway, revealing precise song-related replay fragments. This replay persisted in the absence of NIf input and was dilated in time when we applied a cooling probe to HVC, highlighting the importance of HVC for providing temporal structure for these events. We then lesioned Uva during sleep and found that song-related sequences within HVC remained despite catastrophic changes to singing on the following day. These results support the notion that the HVC microcircuit has sufficient connectivity to sustain sequences in the absence of thalamic feedback, highlighting the value of offline activity for determining the functional structure of neural circuits.

RESULTS

Thalamic lesions eliminate behaviorally relevant network activity

Existing models of HVC circuit organization (Figure 1C-E) differ regarding the role of the polysynaptic feedback loop in sequence production. For instance, thalamic inputs from Uva driven through the feedback loop may be necessary to link individual burst events in HVC (e.g., Figure 1C) or isolated syllable-length sequences (e.g., Figure 1D). We evaluated these possibilities by lesioning Uva and examining the effect of this manipulation on vocal behavior and neural activity in the song system (Schmidt et al., 2004) using high-density silicon probes (Egger et al., 2020). Rather than record sparse premotor activity in HVC, we placed our electrodes into the more densely firing downstream structure RA (Hahnloser et al., 2002; Kozhevnikov and Fee, 2007; Leonardo and Fee, 2005; Yu and Margoliash, 1996) (Figure 1B and 2A-C). Because RA song-related bursts are largely driven by HVC (Figure 2A) (Fee et al., 2004), we used RA activity as an efficient means of monitoring the HVC premotor network.

We found that Uva lesions had a profound impact on both behavior and motor-related activity (Figures 2D-M). In agreement with previous studies (Coleman and Vu, 2005; Danish et al., 2017; Williams and Vicario, 1993), birds were unable to produce normal song following Uva ablation (Figure 2G), though introductory notes – distinct vocalizations which precede song – were considerably less affected (Figures 2F-I). Importantly, song-related bursting events (e.g., Figure 2F) were eliminated following Uva lesions (e.g., Figure 2G, 2J and 2K, proportion of burst spikes: 0.86 ± 0.15 control; 0.02 ± 0.04 lesion).

Instead, RA neurons exhibited regular firing patterns typically found outside the context of vocalization (Figure 2F) (Leonardo and Fee, 2005; Yu and Margoliash, 1996), which are likely the result of intrinsic cellular properties (Mooney, 1992). Unlike burst events, the tonic firing patterns lacked trial-to-trial regularity across vocalizations (control: r = 0.66 ± 0.20; Uva lesion: r = 0.07 ± 0.09) (Figures 2H, 2I, 2L and 2M). These data indicate that, in addition to strongly perturbing singing behavior, lesions to the motor thalamic nucleus Uva result in a complete disappearance of patterned premotor activity during vocal production, rendering us unable to test the previously introduced models regarding the functional organization of HVC (Figure 1C-E).

Robust song-related replay occurs during sleep

To assess the contribution of local circuit connectivity to the propagation of neural sequences, we needed an assay in which the structure of behavior-related network activity could be examined following thalamic ablation. The lack of such dynamics during vocalization prompted us to consider sleep activity, which has been shown to display episodes of burst firing in single neurons resembling patterns observed during singing in the zebra finch (Dave and Margoliash, 2000; Hahnloser et al., 2002; Long et al., 2010). Although singing and sleep are vastly different states whose dynamics are strongly influenced by changes in neuromodulatory tone (Cardin and Schmidt, 2004; Schmidt and Konishi, 1998), the stability of singing (Deregnaucourt et al., 2005; Lombardino and Nottebohm, 2000) and related neural activity (Katlowitz et al., 2018; Rauske et al., 2010) from one day to the next in the adult zebra finch provides the foundation to leverage sleep as a means of examining network organization within the song control pathway.

We used our multielectrode probe to measure activity during singing (Figures 3A and 3B) and sleep (Figures 3C and 3D) in both HVC and RA. Indeed, both regions exhibited population activity during sleep highly resembling that observed during song, supporting the notion that song-related replay is a network-wide event (Fee et al., 2004; Hahnloser and Fee, 2007). We found that RA recordings provided a more precise means of estimating the position of sleep replay events with respect to song (3.2 ± 1.1 ms) than those in HVC (62.5 ± 52.8 ms) (see Methods; Figure 3E) despite having recorded a similar number of neurons in each structure (RA: 52.1 ± 14.8 cells/bird, 8 birds; HVC projection neurons: 49.6 ± 17.6 cells/bird, 5 birds). Distinguishing between our models (Figures 1C-E) requires a highly precise measurement of replayed song activity in the temporal domain (~ 10 ms, or roughly the duration of an HVC burst). We therefore used RA recordings to decode activity in the zebra finch motor pathway during sleep.

We directly compared the activity of RA neurons in 4 birds during sleep and singing by recording for 15.3 ± 2.2 hours, including a continuous dark period (9.7 ± 0.9 hours) when birds spent the majority of time sleeping, and RA exhibited typical ‘sleep bursts’ (Dave and Margoliash, 2000; Hahnloser et al., 2006). We first tested whether individual neurons could be recorded continuously during this period using our high-density recording approach. In addition to our spike sorting protocol (see Methods), the unique electrophysiological properties of RA neurons provided further evidence for recording stability. Because each RA neuron exhibits its own invariant pattern of bursting during vocalization (or temporal

'barcode') (e.g., Figure S1) (Leonardo and Fee, 2005; Yu and Margoliash, 1996), we could directly compare song-related activity before and after the sleep session (Rauske et al., 2010). In all cases, we found the activity of individual RA neurons was preserved (Figure S1), confirming that neurons could be stably recorded throughout the duration of our experiment.

To precisely decode the song content of network activity during sleep, we used a template-matching strategy in which candidate 'replay' sleep epochs (Figure 3D, arrows) – defined by the presence of high-frequency bursts (see Methods) – were discretized into 6 ms bins and compared to population activity recorded during song (Figure S2). Often, sequential bins recorded during sleep closely resembled sequential bins of the song template, allowing us to detect and analyze population-wide sleep replay events (Figures 3F, 3G and S2, see Methods). Population activity during replay events was highly correlated with that observed during song (median: 0.74, interquartile range: 0.65 – 0.83), approaching the degree of regularity observed across different song renditions (median: 0.82, interquartile range: 0.74 – 0.90) and considerably greater than expected by chance (median: 0.00, interquartile range: −0.11 – 0.12) (n = 7 birds) (Figure S2K). A direct comparison of template correlation values reveals that sleep events have 89.9 ± 2.8% of the precision inherent in song events (Figure S2L). Single replay events occurred with a frequency of 11.3 ± 7.9 events/minute (Figure 3H). These events rarely spanned the entire length of the song (range: 0.51 – 0.95 sec) and instead formed shorter sequence fragments (interquartile range: 56 – 140 ms) (Figure 3I) (n = 4 birds).

We observed that the network progressed forward through the song sequence during sleep at nearly the same speed as it does during song itself (replay event slope: 0.96 ± 0.08, n = 26,215 events from 4 birds) (Figure 3J), which is in contrast to the temporally compressed (slope: > 1) and reversed (slope: < 0) replay events observed in the rodent hippocampus (Diba and Buzsaki, 2007; Lee and Wilson, 2002; Wilson and McNaughton, 1994) and consistent with the lack of temporal distortion of replay observed during REM sleep (Louie and Wilson, 2001). Unlike what occurs during song production where sequence start times are limited to syllable boundaries, we found that sleep replay events are initiated throughout the entirety of the song (Figure S3) (88.5 ± 7.7% of analyzed time bins, n = 4 birds). Taken together, these observations demonstrate that replay events in RA during sleep accurately reflect fragments of song-related neural activity, suggesting the circuit architecture responsible for controlling song patterning is engaged during this offline state.

HVC establishes temporal structure for sleep replay

Our study aims to use sleep activity to examine the contribution of local HVC circuit organization to sequence generation (Figure 1). To accomplish this goal, we must ensure that sleep replay in RA is driven by activity within HVC, rather than by dynamics originating within an upstream structure. Previous work used pharmacological inactivation and electrophysiological recordings to conclude that the upstream cortical nucleus NIf may be initiating sleep sequences within HVC (Hahnloser and Fee, 2007). To directly test the role of NIf in sleep replay, we performed excitotoxic lesions within that structure in 2 birds and confirmed the completeness of our manipulation with subsequent histological analysis

(Figure S4A). Although the NIf lesions resulted in transient behavioral abnormalities (Figure S4B) (Cardin et al., 2005; Otchy et al., 2015), we found that robust replay (Figure S4C-G) remained, demonstrating that these dynamics do not require upstream inputs from NIf.

In addition to NIf, several other structures, such as the medial magnocellular nucleus of the anterior neostriatum (Foster et al., 1997; Nottebohm et al., 1976) and the nucleus avalanche (Akutagawa and Konishi, 2010) directly project to HVC and may shape sleep-related activity. To determine the collective contribution of all upstream nuclei to HVC sleep sequences, we measured the impact of mild HVC cooling on replay activity. Previous work has demonstrated that cooling axonal inputs conveying important sequential timing information in a downstream nucleus did not alter the speed of the resultant behavioral sequence (Long and Fee, 2008). Therefore, if a region upstream of HVC were acting as the pattern generator during sleep, we would not expect stretching of sleep-related dynamics upon simply cooling the axon targets within HVC. Alternatively, if the time scale of sleep replay is shaped by local HVC activity, then cooling that structure should measurably slow down replay events (Banerjee et al., 2021).

We distinguish between these possibilities by placing a Peltier device capable of producing graded temperature changes in HVC (ΔT range: 2.8 to 8.7ΔC) while measuring sleep activity in RA (n = 5 birds) (Figure 4). The slope of detected replay events during the cooled periods decreased systematically as a function of HVC temperature (Figures 4A-C) with an average decrease in replay speed of 2.6 ± 1.8 %/°C (Figure 4D), a value consistent with the impact of both induced (Hamaguchi et al., 2016; Long and Fee, 2008) and naturally occurring (Aronov and Fee, 2012) temperature changes on singing behavior. We conclude that HVC dynamics set the tempo for RA replay events, further reinforcing the strategy of testing models of HVC network structure by measuring sleep replay in RA.

Sleep replay events do not require thalamic input

To directly determine the contribution of intrinsic HVC connectivity to sequence propagation, we compared the activity of 134 RA neurons (n = 3 birds) recorded before and after performing overnight electrolytic Uva lesions using a chronically implanted bipolar electrode (Figures 5A, 5B, S5 and S6). If inputs from Uva specifically, or feedback from the song production loop generally, are central to the moment-to-moment burst generation and sequence propagation in the song system (Fig 1C, distributed model), we would expect a significant decrease in sleep bursting and replay events after lesioning, as observed during singing (Figure 2). However, we found that the percentage of spikes in high-frequency bursts did not decrease postlesion (Figures 5A, S5 and S6) (prelesion: 7.5 ± 6.5%, postlesion: 9.7 ± 7.1%; Wilcoxon signed-rank test). To test whether replay was preserved following the Uva lesion, we returned to our template matching strategy (Figures 3 and S2) and measured the incidence of replay events. We found that the frequency (prelesion: 4.1 ± 3.2 events/min, postlesion: 5.4 ± 3.2 events/min; Wilcoxon signed-rank test) and duration (prelesion: 56.3 ± 20.1 ms, postlesion: 62.1 ± 34.0 ms; Wilcoxon rank-sum test) of detected events did not decrease following the lesion (Figures 5B, S5 and S6).

We next examined the fine structure of replay events in the absence of thalamic feedback to HVC by aligning the spiking activity of individual neurons during song and sleep (Figures

5C-F, see Methods). The temporal precision of postlesion sleep activity during replay, defined by similarity to song aligned activity, was consistent with prelesion levels (prelesion: 0.85 ± 0.09, postlesion: 0.82 ± 0.11) (Figure 5G), even though the same neurons no longer exhibited precisely timed bursts during vocalization (Figures 2 and 5H, prelesion: r = 0.66 ± 0.20, postlesion: r = 0.12 ± 0.19). Therefore, despite depriving the network of its thalamic feedback, HVC retained its ability to propagate sequences of song-related activity during sleep, indicating HVC does not require moment-to-moment thalamic input for sequence propagation as described in the distributed model (Figure 1C).

Replay events continue to cross syllable boundaries following thalamic lesion

The retention of patterned bursting activity in the absence of Uva input confirms a role for local HVC circuitry in sequence propagation, which is consistent with the remaining two proposed models. In the subnetwork model (Figure 1D), each vocal element (e.g., syllable) is represented by a distinct HVC circuit which is activated and linked through thalamic feedback (Andalman et al., 2011). This model predicts that following the Uva lesion, replay events should be unable to cross syllable boundaries (Figure 6A). On the other hand, the continuous model, in which the full sequence is reflected in the organization of the HVC circuit, predicts that replay events should not be constrained by the time scales of distinct behavioral units (Figure 6B).

To test these models, we delineated syllable onsets within the corresponding moments of the song template, accounting for the delay between neural activity and vocal onset (Fee et al., 2004) (see Methods). In the absence of thalamic input from Uva, individual replay events continued to cross these boundaries, as in the prelesion period (Figures 6C-D). We estimated the expected boundary crossings according to the subnetwork model by shuffling the syllable order of song templates, which accounts for those crossings that would be expected by chance if independent subnetworks were responsible for each syllable (prelesion: 0.3 ± 0.5%, postlesion: 0.6 ± 0.5%) (Figures 6E and 6F). Instead, we found that replay events crossed syllable boundaries with a frequency much greater than the shuffled estimates (prelesion: 27.1 ± 9.6%, postlesion: 31.1 ± 17.8%) (Figures 6E and 6F). The proportion of crossings for each syllable boundary in the prelesion and postlesion data sets did not differ (Wilcoxon rank-sum test: p = 0.70). The measured slope of the resultant linear regression (0.72, 95% CI [0.43 1.01]) was inconsistent with the subnetwork model (Figure 6G, predicted slope: 0). Instead, our findings support a synaptic architecture in which the HVC microcircuit can produce a single continuous sequence (Figure 6G, predicted slope: 1) representing all song elements (Figure 1E).

DISCUSSION

In this study, we examined the circuit organization of a behaviorally relevant premotor structure underlying song production in the adult zebra finch. To determine the contributions of local and long-range connections to observed dynamics, we lesioned a thalamic node in a feedback pathway critical for song production. In this ‘open loop’ configuration, both behavior and the associated neural activity were severely compromised. We therefore turned to network reactivation during sleep and observed that local HVC circuit connectivity

contains sufficient information to propagate throughout the entirety of the song sequence. Our approach could be instructive for other systems in which the reactivation of behaviorally relevant neural ensembles has been observed during offline states, such as sleep (Gardner et al., 2019; Lee and Wilson, 2002; Trettel et al., 2019; Wilson and McNaughton, 1994) or quiet wakefulness (Diba and Buzsaki, 2007; Foster and Wilson, 2006). Using this strategy, offline circuit examination may become a broadly applicable approach for understanding complex network function, especially in cases where the specific contributions of interdependent structures remain ambiguous (Bolkan et al., 2017; Guo et al., 2017; Sauerbrei et al., 2020; Schmitt et al., 2017).

Our results highlight the importance of local HVC circuit connectivity for sequence generation. Previous work examining the fine structure of HVC network activity suggested a ‘polychronous’ architecture (Egger et al., 2020) in which sequentially active HVC premotor neurons are linked through local axon collaterals (Kornfeld et al., 2017), likely with an additional contribution from HVC inhibitory interneurons (Gibb et al., 2009; Kosche et al., 2015; Markowitz et al., 2015; Wild et al., 2005). We advance this model by indicating that premotor synaptic architecture is capable of continuously representing the entire syllable repertoire of the finch (Figures 1E and 6B). We find that the sequence sustaining circuitry within HVC is not subdivided into dedicated networks related to individual vocal elements, despite the fact that song syllables are functionally (Andalman et al., 2011; Cynx, 1990; Glaze and Troyer, 2006) and developmentally chunked (Lipkind et al., 2017; Okubo et al., 2015). Therefore, in the zebra finch, identified behavioral components (Wiltschko et al., 2015) are not overtly reflected within the functional organization of this critical premotor circuit.

Circuitry within HVC appears to be differentially engaged across singing and sleep. Activity occurring during sleep can be initiated at nearly every time point along the sequence (Figure S3), forming fragmented events. Our observation that sleep replay persists in the absence of NIf raises important questions regarding the factors that initiate these sleep sequences, which may be impacted by sleep-related changes in neuromodulatory tone (Cardin and Schmidt, 2004). In contrast, during singing, the sequence appears to be ballistically engaged at the level of syllables (Cynx, 1990), initiated at a small number of points corresponding to the onsets of vocal elements (Glaze and Troyer, 2006). Although, the mechanisms underlying this process remain unknown, we propose that Uva may be central to this function; the expression of individual behaviors (i.e., syllables) may arise through precisely timed Uva activity (i.e., at syllable onsets) (Danish et al., 2017) and/or through a dedicated thalamocortical pathway onto a subset of HVC premotor neurons capable of initiating the sequences for each vocal element (Andalman et al., 2011; Schmidt, 2003).

The necessity for thalamic input at the level of the syllable may reflect specific requirements for expert song performance. For example, studies using lesions (Williams et al., 1992), cooling (Long and Fee, 2008), and stimulation (Wang et al., 2008) have indicated that neural activity across hemispheres is required for proper song production. In the zebra finch, however, most song control nuclei on the left and right hemispheres (including HVC, RA, NIf, and Uva) do not directly communicate with each other (Schmidt et al., 2004). We therefore propose that bilaterally coordinated brainstem inputs working through

Uva can align the activity of otherwise independent song production systems, thereby ensuring that both hemispheres engage the same part of the sequence (Schmidt, 2003). The requirement of hemispheric coordination during vocal performance could account for the catastrophic impact of Uva lesions on song and the modest (or nonexistent) effects of the same manipulation on sleep when the hemispheres need not be synchronized (Young et al., 2017).

Our results make specific predictions concerning the organization of motor networks in other systems. Although the syntax of the zebra finch is comparatively simple (i.e., invariant syllable order across renditions), we propose a similar network organization in other songbird species that exhibit more variable vocal behavior (Cohen et al., 2020; Fujimoto et al., 2011), with an upstream region playing an important role in determining the order of syllables (Hosino and Okanoya, 2000). While the underlying substrate may be more complex than the continuous representation we observe in the zebra finch, the initiation of discrete local motor programs could be more universal. Future work can determine whether such thalamic engagement of mammalian cortical regions can dynamically coordinate neural assemblies subserving multiple tasks (Dacre et al., 2021; Harvey et al., 2012; Schmitt et al., 2017).

METHODS

RESOURCE AVAILABILITY

Lead contact—Further information and requests for resources and reagents should be directed to and will be fulfilled by the Lead Contact, Michael Long (mlong@med.nyu.edu).

Materials availability—This study did not generate new unique reagents.

Data and Code availability—All code necessary to run template matching as described here can be found at <https://github.com/LongLabGit/TemplateMatching.git> (DOI: 10.5281/zenodo.5500262). The data sets generated during this study and any additional information required to reanalyze the data reported in this paper are available upon request from the Lead Contact.

EXPERIMENTAL MODEL AND SUBJECT DETAILS

We used adult (> 90 days posthatch) male zebra finches (*Taeniopygia guttata*) that were obtained from an outside breeder and maintained in a temperature- and humidity-controlled environment with a 12/12 hr light/dark schedule. All animal maintenance and experimental procedures were performed according to the guidelines established by the Institutional Animal Care and Use Committee at the New York University Langone Medical Center.

METHOD DETAILS

Surgical procedures—All surgical procedures were performed under isoflurane anesthesia (1%–3% in oxygen) following established guidelines. Details pertaining to the use of high-density silicon probes for chronic recordings have been described elsewhere (Egger et al., 2020). Briefly, for all chronic recordings, silicon probes were implanted

directly into the target area using the bifurcation of the sagittal sinus as the stereotaxic origin. For recordings in the robust nucleus of the archipallium (RA) the craniotomies were 2.35 mm lateral and 0.1 mm posterior; for recordings in HVC, the craniotomies were 2.25 mm lateral and 0.25 mm anterior. The ground wire was inserted between the skull and the dura above the cerebellum contralateral to the probe implantation. Silicon elastomer (Kwik-Cast, WPI) was applied to the craniotomy once the target region was successfully identified on all channels (depth: ~2.5–3 mm for RA and 0.5–0.8 mm for HVC) using the Intan Recording system (RHD USB interphase evaluation board or RHD Recording Controller).

For both acute and chronic lesions to Uvaeformis (Uva), coordinates varied from 1.5–1.6 mm lateral, 3.0–3.6 mm anterior and 5.1–5.4 mm ventral. An ipsilateral craniotomy above HVC centered at 2.3 mm lateral and 0.25 mm anterior of the superior sagittal sinus were made for the injection of dextran Alexa Fluor 488 to retrogradely label projections from Uva to HVC allowing for post hoc assessment of lesion success. HVC and Uva craniotomies were done at different head angles: beak bar positioned 45 degrees down from horizontal and 5 degrees up from horizontal for HVC and Uva respectively. Acute lesions were made using custom made bipolar stainless steel electrodes lowered into the Uva craniotomy 24–48 h prior to probe implantation. Both craniotomies were covered with Kwik-Cast (WPI), and the behavioral effects of the lesion were monitored until probe implantation.

For chronic Uva lesions, a platinum-iridium or tungsten search electrode (0.5 MOhm, MicroProbes) was used under isoflurane anesthesia to precisely locate Uva through antidromic activation of HVC-projecting Uva neurons. Next, a custom-built bipolar electrode, composed of a platinum-iridium electrode (0.5 MOhm, MicroProbes) and an insulated stainless steel wire (0.002”, California Fine Wire) was lowered into Uva and secured with dental acrylic. The uninsulated tip of the stainless steel wire and the tip of the platinum-iridium electrode were ~ 400 μm apart. Birds recovered from implantation surgery and were monitored to ensure no disruptions to song production following bipolar electrode implantation. Lesions were performed in the middle of the dark period following silicon probe implantation. For both acute and chronic lesion approaches the implantation of silicon probes was carried out as described above, and electrolytic lesions were achieved with 30 second biphasic pulses (acute: 50 μA, 6 total pulses; chronic: 50–500 μA, 6–10 total pulses).

NIf lesions were performed using the excitotoxin *N*-methyl-DL-aspartic acid (NMA, 4%), as described previously (Otchy et al., 2015). The extent and exact position of NIf was mapped using a 0.5 MΩ tungsten electrode (MicroProbes, WE30030.5B3) to measure antidromic responses evoked by a stainless steel bipolar electrode in HVC that was constructed from 50 μm Teflon coated stainless steel wire (California Fine Wire). NMA injections (12 sites, 30 nL each. 200 μm spacing) were then made along the anterior-posterior axis of NIf. Prior to application of NMA, dextran was injected into HVC (see Uva lesion protocol) to retrogradely label HVC-projecting NIf and Uva neurons. Following surgery, all vocalizations were recorded until song recovered to prelesion performance (Cardin et al., 2005; Otchy et al., 2015), at which time high-density silicon probes were implanted into RA.

Extracellular Recordings—Chronic recordings were performed using integrated 128-channel high-density silicon probes (Diagnostic Biochips, 128–5). Prior to surgery, integrated probes were mounted to a microdrive (NeuroNexus, d-XL) and a stainless steel ground wire (0.001” AM systems) was soldered to the reference of the headstage, which was held in place by a custom-made 3D printed enclosure (Formlabs). Within the hour following surgery, we began continuously recording neural activity from RA (Intan Recording Controller) and all vocalizations using an omnidirectional microphone (Audio Technica) and an analog preamplifier (Presonus). Free movement was enabled by an electrically assisted commutator (Doric Lenses). Female zebra finches were placed in an adjacent cage to elicit song. In a subset of experiments, electrolytic lesions were performed following 3–6 hours of sleep.

Focal Cooling—Cooling experiments required a preparatory surgery, during which a small stainless steel headplate was secured to the anterior-most position on the skull. A small craniotomy and durotomy were made for access to RA 2.3 mm lateral and 1.8 mm posterior to the superior sagittal sinus, and a large craniotomy 2 mm medial-lateral x 1.3 mm anterior-posterior centered on HVC was made to accommodate the cooling device as described previously (Long and Fee, 2008).

For the cooling experiments, birds were head-fixed and held in a foam restraint prior to recording. At the beginning of the recording session, a Peltier device (Custom Thermoelectric) was lowered onto the surface of the brain within the HVC craniotomy. This device was wired to a power source (Kepko) that allowed for careful control of applied current. A thin copper pouch whose temperature was maintained through flowing water was used as a heat sink (Long and Fee, 2008). Next, 128-channel acute high-density silicon probes (S. Masmanidis, UCLA; 128-K) (Yang et al., 2020) were lowered into the RA craniotomy. The temperature was varied in a block fashion (~1 hour per condition) with a return to baseline temperature between each cooling session. Following recording, a thermocouple probe (Omega) was inserted into HVC (depth: 0.5 mm) to measure the temperature changes resulting from each current level administered during the experiment.

Histology—After recording, birds were perfused with 4% PFA and probes were recovered. Brains were fixed overnight and sliced at 50–100 μm using a vibrating microtome (VT1200S, Leica). Slices were mounted (Vectashield) and imaged using a Zeiss Confocal microscope (LSM800).

DATA ANALYSIS

Recording neural activity during song—Custom MATLAB software was used to analyze song recordings and to align single unit data to behavior. To characterize song elements, the audio signal was bandpass filtered (low freq. = 500 Hz, high freq. = 8 kHz) and down sampled to 300 Hz to extract the amplitude envelope. This signal was then divided into three second segments; those segments with amplitude above of the noise floor for greater than 30 samples were assessed for vocal content. The start and stop times of all male vocalizations in these segments as well as the identity of the vocalization (i.e., syllable A, introductory note, call) were manually annotated.

For electrophysiological recordings, automated spike detection and sorting was carried out using Kilosort software (Pachitariu et al., 2016) and manual post-processing was performed using Phy (Rossant et al., 2016) as described previously (Egger et al., 2020). To confirm that we were holding the same neurons throughout our recording, in addition to amplitude and waveform stability (Phy), we compared singing activity in a subset of birds where song was recorded before (day 1) and after (day 2) sleep. For each bird, we calculated the Pearson correlation between the average song-related instantaneous firing rate on day 1 and day 2 for each neuron after aligning all song-related activity to the beginning and end of the song motif.

Both singing and sleep replay are associated with high frequency burst firing in the song production pathway. For each neuron, we calculated the percent of spikes within all song-related vocalizations belonging to a burst (instantaneous firing rate: > 100 Hz) within the window of vocal production after accounting for a 15 ms motor delay (Fee et al., 2004). Vocalizations defined as ‘song-related’ included both introductory notes and either song syllables (intact: control and chronic prelesion) or song attempts (postlesion: acute lesion and chronic postlesion) and excluded calls. To measure spiking precision during vocalizations, all spikes occurring within introductory notes were aligned to the warped start and stop times of each vocalization. The instantaneous firing rates for each aligned trial were smoothed with a 10 ms boxcar kernel and compared within condition (intact or postlesion) using the Pearson correlation. This firing rate threshold and smoothing procedure was used for all instantaneous firing rate measurements throughout the study.

To calculate temporal uncertainty, we compared song-related RA data collected as part of this study with a previously acquired HVC data set (Egger et al., 2020). The population activity during song was temporally subsampled every 2 ms and the probability of a given unique active neural ensemble was used to calculate entropy (I) (Leonardo and Fee, 2005); uncertainty was then defined as song length divided by 2^I for each recording.

Template matching—A single template was chosen from the burst activity of the population of RA neurons during the performance of one song rendition and subdivided into bins (bin width: 6 ms, step size: 2 ms). The data were then further binarized; if a neuron was bursting within that bin, it was assigned a value of 1; no bursting was assigned a 0. Following the creation of the template, activity throughout the recording period was similarly binarized, segmented into bins, and assigned to the template bin it most resembles using Pearson correlation.

Sleep replay events were defined as fragments of sleep activity resembling significant portions of the song template using the following guidelines during the lights-off portion of the recording. Individual replay events were detected by traversing the two-dimensional space (template bin vs. recording time); a given bin assignment was joined with its neighbor if the absolute value of the distance between them was less than 4 ms, thus allowing for the detection of both forward and reverse replay events. Adjacent detected events were joined if the distance between them was less than 10 ms.

We calculated the slope of each event using a best fit linear approximation of the bin assignments within the detected event. Initial manual annotation of robust replay events suggested that most slope values were near 1. We therefore used outlier slope values (less than 0 and greater than 2) as a means of identifying spurious events. Using this metric, we found that replay events of sufficient length (i.e., 40 ms) very rarely exhibited an outlier slope value (Figure S2G), and we therefore established 40 ms as a minimum requirement for sleep replay events upon which we performed further analysis. We estimated the spectrogram of sleep replay events by assigning the portion of the song spectrogram corresponding to the template bin with the highest correlation value. For the cooling experiments, where no song template was available, we created a template from a period of robust bursting during a baseline temperature recording block, and slopes for the events detected during the cooled portions were normalized to the median slope of the detected baseline events.

To compare the similarity between song activity and sleep replay activity, we looked at the template matching results for detected sleep replay events as well as the non-template song repeats (i.e., the neural activity occurring during song renditions not used for the template). We compared all correlation scores assigned during non-template song repeats with those assigned during sleep events. We produced a shuffled distribution of correlation scores by comparing the neural activity during non-template song repeats and detected replay events to random portions of the song (rather than the winner-take-all approach used for event detection). We also performed a direct comparison in which we measured the correlation scores across sleep and song for each bin of our template, using the mean values for each bird to calculate a ratio (i.e., r_{sleep}/r_{song}).

Sleep activity and replay measurements—Population bursting during sleep was measured as the percent of all spikes occurring within a burst (instantaneous firing rate: > 100Hz; bin width: 1 minute). To compare spiking precision within detected replay events pre- and postlesion, template matching was performed on neural data collected during awake singing trials. All spiking activity for a given neuron was aligned to all the detected events during song, prelesion replay, and postlesion replay. Average instantaneous firing rates for pre- and postlesion replay activity were compared to that of singing activity (Pearson correlation). To quantify potential differences in replay events before and after the lesion, we narrowed our analysis to the hour preceding the lesion (prelesion) and the second hour following the lesion (postlesion).

Syllable boundary crossings—All detected sleep replay events were assessed for boundary crossing by comparing the event's template location with the corresponding position in song. A syllable was defined as the onset of the vocalization to the onset of the following syllable vocalization or the end of that vocalization for the last syllable in the song. Replay event starting times were normalized to their location within the starting syllable and stop times were adjusted to the position in the ending syllable. We also quantify the proportion of reconstructed replay events that cross syllable boundaries (e.g., sleep events initiated in syllable A that cross over into syllable B). To create replay events predicted by the subnetwork model, we shuffled the template such that the corresponding

neural activity for each syllable remained intact, but that previously adjacent syllables were no longer continuous. For each bird, we generated either ten such templates meeting this criterion or all shuffled templates when fewer than ten were possible. Using the shuffled template bin assignments, events were detected and syllable boundary crossings were measured as above.

QUANTIFICATION AND STATISTICAL ANALYSIS

All statistical details of experiments can be found in figure legends and the Results section, including the statistical tests used, exact value of n and what n represents (e.g., number of animals, number of cells, etc.). Values are reported as mean ± SD unless mentioned otherwise, and values are plotted as mean with error bars representing SD unless mentioned otherwise. Significance was defined at a level of 0.05. Normal distribution of data was not assumed. No data were excluded from analysis. Statistical calculations were performed using MATLAB R2017a.

Supplementary Material

Refer to Web version on PubMed Central for supplementary material.

ACKNOWLEDGEMENTS

This research was supported by NIH F31 NS116933–01 (M.E.), NIH R01 NS075044 (M.A.L.), and Simons Global Brain (M.A.L.). We thank Arkarup Banerjee, György Buzsáki, Dezhe Jin, Katherine Nagel, and members of the Long laboratory for comments on earlier versions of this manuscript. Ralph Peterson helped with data collection, and Abby Paulson provided technical assistance. We acknowledge helpful conversations with Robert Egger, Liam Paninski, Josh Glaser, and Erdem Varol.

REFERENCES

Akutagawa E, and Konishi M (2010). New brain pathways found in the vocal control system of a songbird. J Comp Neurol 518, 3086–3100. [PubMed: 20533361]

Andalman AS, Foerster JN, and Fee MS (2011). Control of vocal and respiratory patterns in birdsong: dissection of forebrain and brainstem mechanisms using temperature. PLoS One 6, e25461. [PubMed: 21980466]

Aronov D, and Fee MS (2012). Natural changes in brain temperature underlie variations in song tempo during a mating behavior. PLoS One 7, e47856. [PubMed: 23112858]

Banerjee A, Egger R, and Long MA (2021). Using focal cooling to link neural dynamics and behavior. Neuron

Bolkan SS, Stujenske JM, Parnaudeau S, Spellman TJ, Rauffenbart C, Abbas AI, Harris AZ, Gordon JA, and Kellendonk C (2017). Thalamic projections sustain prefrontal activity during working memory maintenance. Nat Neurosci 20, 987–996. [PubMed: 28481349]

Cardin JA, Raksin JN, and Schmidt MF (2005). Sensorimotor nucleus NIf is necessary for auditory processing but not vocal motor output in the avian song system. J Neurophysiol 93, 2157–2166. [PubMed: 15590726]

Cardin JA, and Schmidt MF (2004). Noradrenergic inputs mediate state dependence of auditory responses in the avian song system. J Neurosci 24, 7745–7753. [PubMed: 15342742]

Cohen Y, Shen J, Semu D, Leman DP, Liberti WA 3rd, Perkins LN, Liberti DC, Kotton DN, and Gardner TJ (2020). Hidden neural states underlie canary song syntax. Nature 582, 539–544. [PubMed: 32555461]

Coleman MJ, and Mooney R (2004). Synaptic transformations underlying highly selective auditory representations of learned birdsong. J Neurosci 24, 7251–7265. [PubMed: 15317851]

Coleman MJ, and Vu ET (2005). Recovery of impaired songs following unilateral but not bilateral lesions of nucleus uvaeformis of adult zebra finches. J Neurobiol 63, 70–89. [PubMed: 15685609]

Cynx J (1990). Experimental determination of a unit of song production in the zebra finch (Taeniopygia guttata). J Comp Psychol 104, 3–10. [PubMed: 2354628]

Dacre J, Colligan M, Clarke T, Ammer JJ, Schiemann J, Chamosa-Pino V, Claudi F, Harston JA, Eleftheriou C, Pakan JMP, et al. (2021). A cerebellar-thalamocortical pathway drives behavioral context-dependent movement initiation. Neuron 109, 2326–2338 e2328. [PubMed: 34146469]

Danish HH, Aronov D, and Fee MS (2017). Rhythmic syllable-related activity in a songbird motor thalamic nucleus necessary for learned vocalizations. PLoS One 12, e0169568. [PubMed: 28617829]

Dave AS, and Margoliash D (2000). Song replay during sleep and computational rules for sensorimotor vocal learning. Science 290, 812–816. [PubMed: 11052946]

Deregnaucourt S, Mitra PP, Feher O, Pytte C, and Tchernichovski O (2005). How sleep affects the developmental learning of bird song. Nature 433, 710–716. [PubMed: 15716944]

Diba K, and Buzsaki G (2007). Forward and reverse hippocampal place-cell sequences during ripples. Nat Neurosci 10, 1241–1242. [PubMed: 17828259]

Egger R, Tupikov Y, Elmaleh M, Katlowitz KA, Benezra SE, Picardo MA, Moll F, Kornfeld J, Jin DZ, and Long MA (2020). Local Axonal Conduction Shapes the Spatiotemporal Properties of Neural Sequences. Cell 183, 537–548 e512. [PubMed: 33064989]

Fee MS, Kozhevnikov AA, and Hahnloser RH (2004). Neural mechanisms of vocal sequence generation in the songbird. Ann N Y Acad Sci 1016, 153–170. [PubMed: 15313774]

Foster DJ, and Wilson MA (2006). Reverse replay of behavioural sequences in hippocampal place cells during the awake state. Nature 440, 680–683. [PubMed: 16474382]

Foster EF, Mehta RP, and Bottjer SW (1997). Axonal connections of the medial magnocellular nucleus of the anterior neostriatum in zebra finches. J Comp Neurol 382, 364–381. [PubMed: 9183699]

Fujimoto H, Hasegawa T, and Watanabe D (2011). Neural coding of syntactic structure in learned vocalizations in the songbird. J Neurosci 31, 10023–10033. [PubMed: 21734294]

Galvis D, Wu W, Hyson RL, Johnson F, and Bertram R (2017). A distributed neural network model for the distinct roles of medial and lateral HVC in zebra finch song production. J Neurophysiol 118, 677–692. [PubMed: 28381490]

Gardner RJ, Lu L, Wernle T, Moser MB, and Moser EI (2019). Correlation structure of grid cells is preserved during sleep. Nat Neurosci 22, 598–608. [PubMed: 30911185]

Gibb L, Gentner TQ, and Abarbanel HD (2009). Inhibition and recurrent excitation in a computational model of sparse bursting in song nucleus HVC. J Neurophysiol 102, 1748–1762. [PubMed: 19515949]

Glaze CM, and Troyer TW (2006). Temporal structure in zebra finch song: implications for motor coding. J Neurosci 26, 991–1005. [PubMed: 16421319]

Guo ZV, Inagaki HK, Daie K, Druckmann S, Gerfen CR, and Svoboda K (2017). Maintenance of persistent activity in a frontal thalamocortical loop. Nature 545, 181–186. [PubMed: 28467817]

Hahnloser RH, and Fee MS (2007). Sleep-related spike bursts in HVC are driven by the nucleus interface of the nidopallium. J Neurophysiol 97, 423–435. [PubMed: 17005618]

Hahnloser RH, Kozhevnikov AA, and Fee MS (2002). An ultra-sparse code underlies the generation of neural sequences in a songbird. Nature 419, 65–70. [PubMed: 12214232]

Hahnloser RH, Kozhevnikov AA, and Fee MS (2006). Sleep-related neural activity in a premotor and a basal-ganglia pathway of the songbird. J Neurophysiol 96, 794–812. [PubMed: 16495362]

Hahnloser RH, Wang CZ, Nager A, and Naie K (2008). Spikes and bursts in two types of thalamic projection neurons differentially shape sleep patterns and auditory responses in a songbird. J Neurosci 28, 5040–5052. [PubMed: 18463257]

Hamaguchi K, Tanaka M, and Mooney R (2016). A Distributed Recurrent Network Contributes to Temporally Precise Vocalizations. Neuron 91, 680–693. [PubMed: 27397518]

Harvey CD, Coen P, and Tank DW (2012). Choice-specific sequences in parietal cortex during a virtual-navigation decision task. Nature 484, 62–68. [PubMed: 22419153]

Hosino T, and Okanoya K (2000). Lesion of a higher-order song nucleus disrupts phrase level complexity in Bengalese finches. Neuroreport 11, 2091–2095. [PubMed: 10923650]

Katlowitz KA, Picardo MA, and Long MA (2018). Stable Sequential Activity Underlying the Maintenance of a Precisely Executed Skilled Behavior. Neuron 98, 1133–1140 e1133. [PubMed: 29861283]

Kornfeld J, Benezra SE, Narayanan RT, Svara F, Egger R, Oberlaender M, Denk W, and Long MA (2017). EM connectomics reveals axonal target variation in a sequence-generating network. Elife 6.

Kosche G, Vallentin D, and Long MA (2015). Interplay of inhibition and excitation shapes a premotor neural sequence. J Neurosci 35, 1217–1227. [PubMed: 25609636]

Kozhevnikov AA, and Fee MS (2007). Singing-related activity of identified HVC neurons in the zebra finch. J Neurophysiol 97, 4271–4283. [PubMed: 17182906]

Lee AK, and Wilson MA (2002). Memory of sequential experience in the hippocampus during slow wave sleep. Neuron 36, 1183–1194. [PubMed: 12495631]

Leonardo A, and Fee MS (2005). Ensemble coding of vocal control in birdsong. J Neurosci 25, 652–661. [PubMed: 15659602]

Lipkind D, Zai AT, Hanuschkin A, Marcus GF, Tchernichovski O, and Hahnloser RHR (2017). Songbirds work around computational complexity by learning song vocabulary independently of sequence. Nat Commun 8, 1247. [PubMed: 29089517]

Lombardino AJ, and Nottebohm F (2000). Age at deafening affects the stability of learned song in adult male zebra finches. J Neurosci 20, 5054–5064. [PubMed: 10864963]

Long MA, and Fee MS (2008). Using temperature to analyse temporal dynamics in the songbird motor pathway. Nature 456, 189–194. [PubMed: 19005546]

Long MA, Jin DZ, and Fee MS (2010). Support for a synaptic chain model of neuronal sequence generation. Nature 468, 394–399. [PubMed: 20972420]

Louie K, and Wilson MA (2001). Temporally structured replay of awake hippocampal ensemble activity during rapid eye movement sleep. Neuron 29, 145–156. [PubMed: 11182087]

Lynch GF, Okubo TS, Hanuschkin A, Hahnloser RH, and Fee MS (2016). Rhythmic Continuous-Time Coding in the Songbird Analog of Vocal Motor Cortex. Neuron 90, 877–892. [PubMed: 27196977]

MacDonald CJ, Lepage KQ, Eden UT, and Eichenbaum H (2011). Hippocampal “time cells” bridge the gap in memory for discontiguous events. Neuron 71, 737–749. [PubMed: 21867888]

Mackevicius EL, Happ MTL, and Fee MS (2020). An avian cortical circuit for chunking tutor song syllables into simple vocal-motor units. Nat Commun 11, 5029. [PubMed: 33024101]

Markowitz JE, Liberti WA 3rd, Guitchounts G, Velho T, Lois C, and Gardner TJ (2015). Mesoscopic patterns of neural activity support songbird cortical sequences. PLoS Biol 13, e1002158. [PubMed: 26039895]

Mooney R (1992). Synaptic basis for developmental plasticity in a birdsong nucleus. J Neurosci 12, 2464–2477. [PubMed: 1351935]

Mooney R, and Prather JF (2005). The HVC microcircuit: the synaptic basis for interactions between song motor and vocal plasticity pathways. J Neurosci 25, 1952–1964. [PubMed: 15728835]

Nottebohm F, Stokes TM, and Leonard CM (1976). Central control of song in the canary, Serinus canarius. J Comp Neurol 165, 457–486. [PubMed: 1262540]

Okubo TS, Mackevicius EL, Payne HL, Lynch GF, and Fee MS (2015). Growth and splitting of neural sequences in songbird vocal development. Nature 528, 352–357. [PubMed: 26618871]

Otchy TM, Wolff SB, Rhee JY, Pehlevan C, Kawai R, Kempf A, Gobes SM, and Olveczky BP (2015). Acute off-target effects of neural circuit manipulations. Nature 528, 358–363. [PubMed: 26649821]

Pachitariu M, Steinmetz N, Kadir S, Carandini M, and Kenneth D, H. (2016). Kilosort: realtime spike-sorting for extracellular electrophysiology with hundreds of channels. bioRxiv, 061481.

Pastalkova E, Itskov V, Amarasingham A, and Buzsaki G (2008). Internally generated cell assembly sequences in the rat hippocampus. Science 321, 1322–1327. [PubMed: 18772431]

Peters AJ, Chen SX, and Komiyama T (2014). Emergence of reproducible spatiotemporal activity during motor learning. Nature 510, 263–267. [PubMed: 24805237]

Picardo MA, Merel J, Katlowitz KA, Vallentin D, Okobi DE, Benezra SE, Clary RC, Pnevmatikakis EA, Paninski L, and Long MA (2016). Population-Level Representation of a Temporal Sequence Underlying Song Production in the Zebra Finch. Neuron 90, 866–876. [PubMed: 27196976]

Rauske PL, Chi Z, Dave AS, and Margoliash D (2010). Neuronal stability and drift across periods of sleep: premotor activity patterns in a vocal control nucleus of adult zebra finches. J Neurosci 30, 2783–2794. [PubMed: 20164361]

Reinke H, and Wild JM (1998). Identification and connections of inspiratory premotor neurons in songbirds and budgerigar. J Comp Neurol 391, 147–163. [PubMed: 9518266]

Roberts TF, Gobes SM, Murugan M, Olveczky BP, and Mooney R (2012). Motor circuits are required to encode a sensory model for imitative learning. Nat Neurosci 15, 1454–1459. [PubMed: 22983208]

Rossant C, Kadir SN, Goodman DFM, Schulman J, Hunter MLD, Saleem AB, Grosmark A, Belluscio M, Denfield GH, Ecker AS, et al. (2016). Spike sorting for large, dense electrode arrays. Nat Neurosci 19, 634–641. [PubMed: 26974951]

Sauerbrei BA, Guo JZ, Cohen JD, Mischiati M, Guo W, Kabra M, Verma N, Mensh B, Branson K, and Hantman AW (2020). Cortical pattern generation during dexterous movement is input-driven. Nature 577, 386–391. [PubMed: 31875851]

Schmidt MF (2003). Pattern of interhemispheric synchronization in HVc during singing correlates with key transitions in the song pattern. J Neurophysiol 90, 3931–3949. [PubMed: 12944542]

Schmidt MF, Ashmore RC, and Vu ET (2004). Bilateral control and interhemispheric coordination in the avian song motor system. Ann N Y Acad Sci 1016, 171–186. [PubMed: 15313775]

Schmidt MF, and Konishi M (1998). Gating of auditory responses in the vocal control system of awake songbirds. Nat Neurosci 1, 513–518. [PubMed: 10196550]

Schmitt LI, Wimmer RD, Nakajima M, Happ M, Mofakham S, and Halassa MM (2017). Thalamic amplification of cortical connectivity sustains attentional control. Nature 545, 219–223. [PubMed: 28467827]

Scotto-Lomassese S, Rochefort C, Nshdejan A, and Scharff C (2007). HVC interneurons are not renewed in adult male zebra finches. Eur J Neurosci 25, 1663–1668. [PubMed: 17408434]

Skaggs WE, McNaughton BL, Wilson MA, and Barnes CA (1996). Theta phase precession in hippocampal neuronal populations and the compression of temporal sequences. Hippocampus 6, 149–172. [PubMed: 8797016]

Striedter GF, and Vu ET (1998). Bilateral feedback projections to the forebrain in the premotor network for singing in zebra finches. J Neurobiol 34, 27–40. [PubMed: 9469616]

Tchernichovski O, Mitra PP, Lints T, and Nottebohm F (2001). Dynamics of the vocal imitation process: how a zebra finch learns its song. Science 291, 2564–2569. [PubMed: 11283361]

Trettel SG, Trimper JB, Hwaun E, Fiete IR, and Colgin LL (2019). Grid cell co-activity patterns during sleep reflect spatial overlap of grid fields during active behaviors. Nat Neurosci 22, 609–617. [PubMed: 30911183]

Wang CZ, Herbst JA, Keller GB, and Hahnloser RH (2008). Rapid interhemispheric switching during vocal production in a songbird. PLoS Biol 6, e250. [PubMed: 18922044]

Wild JM (1993). Descending projections of the songbird nucleus robustus archistriatalis. J Comp Neurol 338, 225–241. [PubMed: 8308169]

Wild JM, Williams MN, Howie GJ, and Mooney R (2005). Calcium-binding proteins define interneurons in HVC of the zebra finch (Taeniopygia guttata). J Comp Neurol 483, 76–90. [PubMed: 15672397]

Williams H, Crane LA, Hale TK, Esposito MA, and Nottebohm F (1992). Right-side dominance for song control in the zebra finch. J Neurobiol 23, 1006–1020. [PubMed: 1460461]

Williams H, and Vicario DS (1993). Temporal patterning of song production: participation of nucleus uvaeformis of the thalamus. J Neurobiol 24, 903–912. [PubMed: 8228968]

Wilson MA, and McNaughton BL (1994). Reactivation of hippocampal ensemble memories during sleep. Science 265, 676–679. [PubMed: 8036517]

Wiltschko AB, Johnson MJ, Iurilli G, Peterson RE, Katon JM, Pashkovski SL, Abraira VE, Adams RP, and Datta SR (2015). Mapping Sub-Second Structure in Mouse Behavior. Neuron 88, 1121–1135. [PubMed: 26687221]

Yang L, Lee K, Villagracia J, and Masmanidis SC (2020). Open source silicon microprobes for high throughput neural recording. J Neural Eng 17, 016036. [PubMed: 31731284]

Young BK, Mindlin GB, Arneodo E, and Goller F (2017). Adult zebra finches rehearse highly variable song patterns during sleep. PeerJ 5, e4052. [PubMed: 29158983]

Yu AC, and Margoliash D (1996). Temporal hierarchical control of singing in birds. Science 273, 1871–1875. [PubMed: 8791594]

Zhao W, Garcia-Oscos F, Dinh D, and Roberts TF (2019). Inception of memories that guide vocal learning in the songbird. Science 366, 83–89. [PubMed: 31604306]

Highlights:

- Thalamic lesions eliminate singing behavior and underlying network dynamics
- High-density recordings during song enable precise decoding of sleep replay
- Temporal dynamics during sleep are controlled by premotor nucleus HVC
- Structure of sleep replay events highlights role of local HVC connectivity

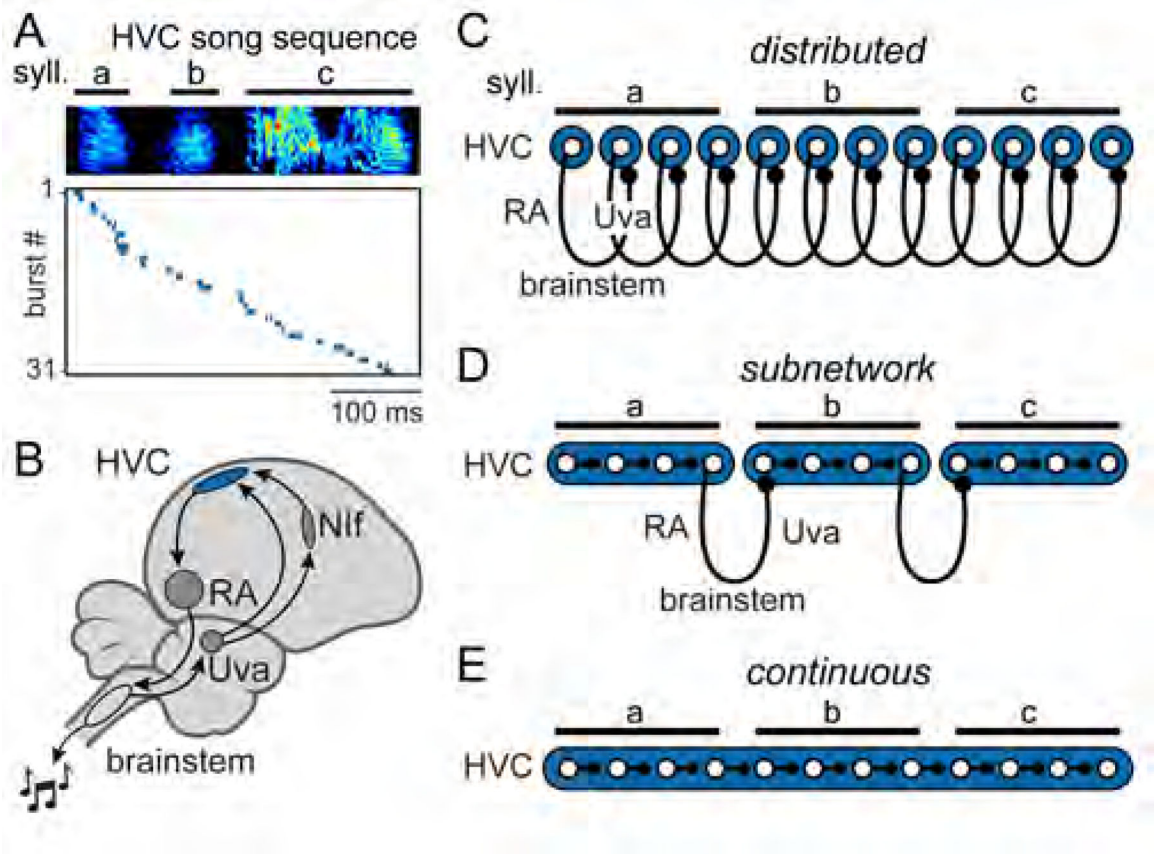

Figure 1. Models of premotor sequence generation

(A) Activity of simultaneously recorded HVC projection neurons during singing (top: song spectrogram) in an adult zebra finch (n = 31 burst events). HVC recordings replotted from a previous data set (Egger et al., 2020).

(B) Zebra finch song control system, including HVC (proper name), robust nucleus of the arcopallium (RA), nucleus Uvaeformis (Uva), and nucleus interfacialis of the nidopallium (NIf).

(C-E) Three models of HVC organization. *Distributed model*: HVC local connectivity is not capable of moment-to-moment sequence propagation. *Subnetwork model*: HVC is functionally divided into discrete subnetworks. *Continuous model*: local connectivity is sufficient to link sequentially active neurons throughout the duration of the song.

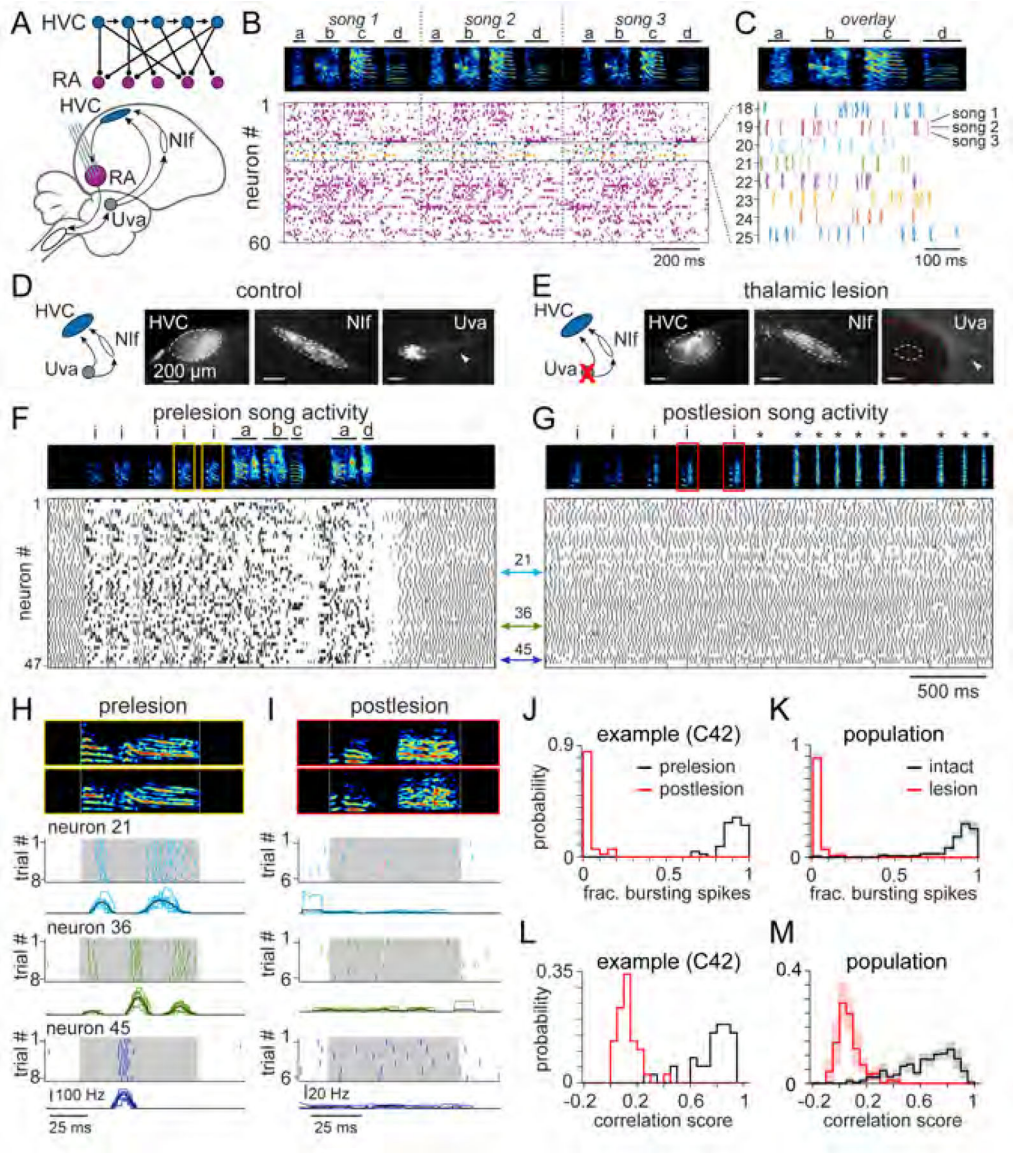

Figure 2. Thalamic lesions eliminate motor-related signals in the song production pathway

(A) Recordings in panels (B), (C), (F) – (I) performed within RA, a downstream target of HVC. Schematic (adapted from Fee et al., 2004) depicts the transformation of the sparse HVC sequence to a dense RA representation due to synaptic convergence.

(B) Spiking activity from 60 simultaneously recorded RA neurons during three successive songs.

(C) Song-aligned spiking activity from 8 example neurons in (B).

(D and E) Retrogradely labeled cell bodies in NIf and Uva following dextran injection into HVC in intact (D) and Uva-lesioned (E) brains. White arrows highlight Uva axons. Red dashed line in (E) shows lesion border. White dashed line represents estimated location of Uva before lesion.

(F and G) (Top) Annotated spectrograms of vocalizations before (F) and after (G) lesion for Bird C42 (i: introductory note, *: attempted song vocalizations). (Bottom) Spiking activity

for 47 simultaneously recorded RA neurons. Spectrogram elements representing cage noise and female vocalizations were removed post-hoc for visual clarity.

(H and I) (Top) Two example introductory notes from Bird C42, expanded from yellow and red boxes in (F) and (G), respectively. (Bottom) Introductory note aligned spike rasters before (H) and after (I) Uva lesion. Instantaneous firing rate for all trials shown below. Black line: mean. White dashed lines (top) and gray shaded region (bottom) indicate duration of vocal element.

(J) Fraction of song-related spikes meeting burst criteria for Bird C42 ($n = 47$ neurons) before (black) and after (red) Uva lesion (Wilcoxon sign rank: $p < 0.0001$).

(K) Population data of the fraction of song-related spikes meeting burst criteria for 10 intact birds ($n = 445$ neurons, 49.4 ± 16 neurons per bird) and 6 Uva lesioned birds ($n = 375$ neurons, 62.5 ± 27 neurons per bird) (Wilcoxon rank sum test: $p < 0.0001$).

(L) Average Pearson correlation scores across instantaneous firing rates during introductory notes for Bird C42 (Wilcoxon sign rank: $p < 0.0001$).

(M) Population data of average Pearson correlation scores during introductory notes for 10 intact birds ($n = 399$ neurons) and 6 Uva lesioned birds ($n = 344$ neurons; Wilcoxon rank sum: $p < 0.0001$). (L and M) Neurons with fewer than two spikes on average per trial were excluded from this analysis. (K and M) Histograms show mean ± SEM.

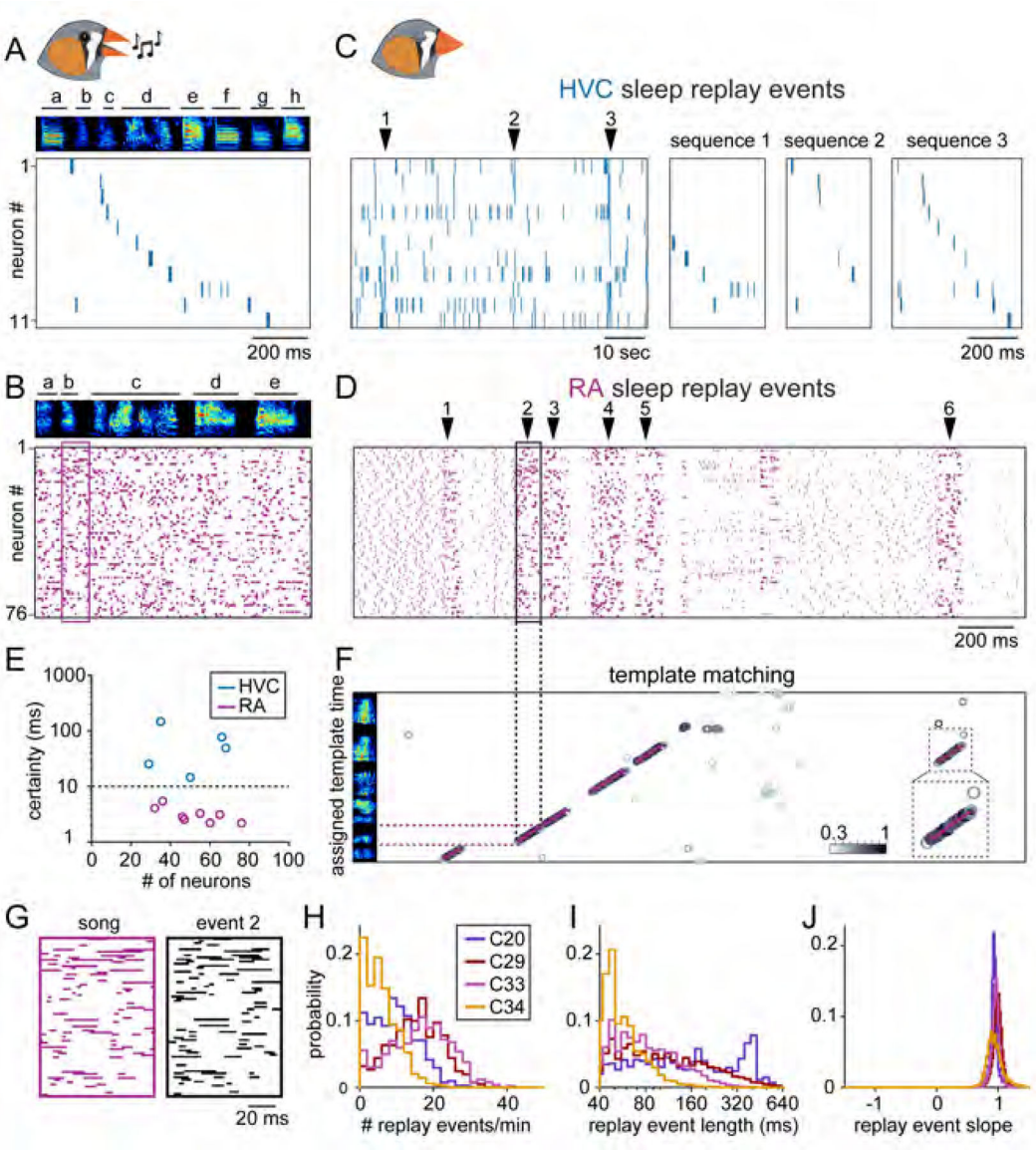

Figure 3. Song-related activity during sleep in HVC and RA

(A-D) Simultaneously recorded spiking activity of 11 HVC projection neurons and 76 RA neurons during song (A and B) and sleep (C and D). Arrows in (C) indicate position of example replay sequences to the right.

(E) Temporal certainty from 8 RA (magenta) and 5 HVC (blue) data sets (see Methods). Dashed line (10 ms) represents the threshold for testing functional models described in Figure 1.

(F) Template matching applied to RA activity in (D). Each data point is aligned to the assigned bin of song template (y-axis) and color indicates Pearson correlation score. Detected events fitted by purple line. Inset: template matching results from event 6 (indicated by black dashed square).

(G) Binarized bursting activity for replay event 2 from (D) compared with the assigned fragment of the song from (B).

(H-J) Characterization of replay event frequency during each 1-minute period of the recording (H) as well as the replay length (I) and slope (J) for 4 birds.
See also Figure S1-S3.

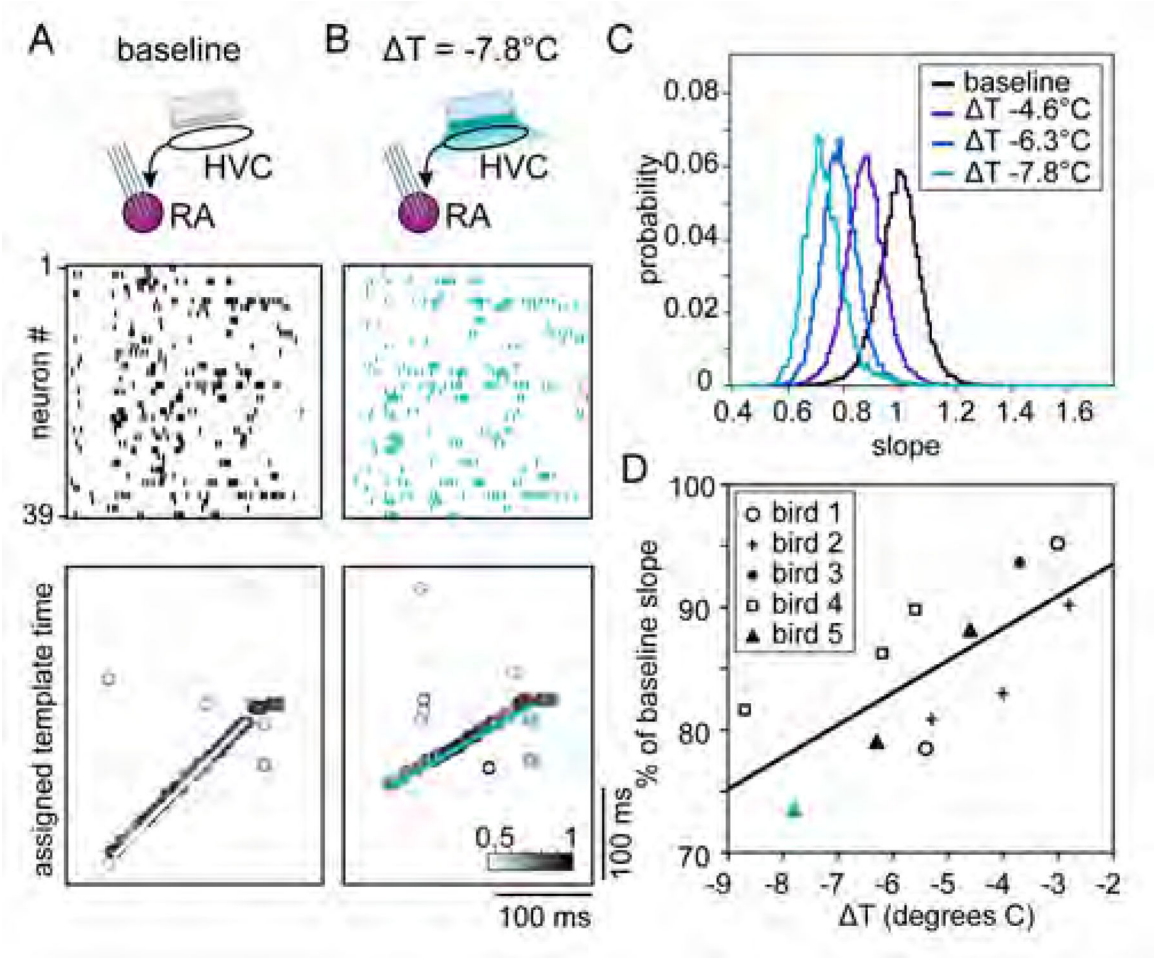

Figure 4. Focal HVC cooling slows sleep replay events in RA

(A and B) (Top) Schematic of experiment, with silicon probes in RA and a Peltier device on the surface of HVC. Spiking activity (middle) and template matching results (bottom) for 39 simultaneously recorded RA neurons in the baseline (A) and cooled (B) conditions. Detected example events for baseline and cooled conditions shown in white (A) and teal (B), respectively.

(C) Distribution of slopes for each temperature condition in Bird 5 normalized to the mean baseline (ΔT = 0°C) slope.

(D) Population data for all birds (n = 5); each data point indicates the mean slope relative to baseline for a given condition in a single bird. Teal triangle is maximum cooling condition from (C) (ΔT = −7.8°C). Best fit line: slope = 2.6%/°C; $R^2 = 0.51$.

See also Figure S4.

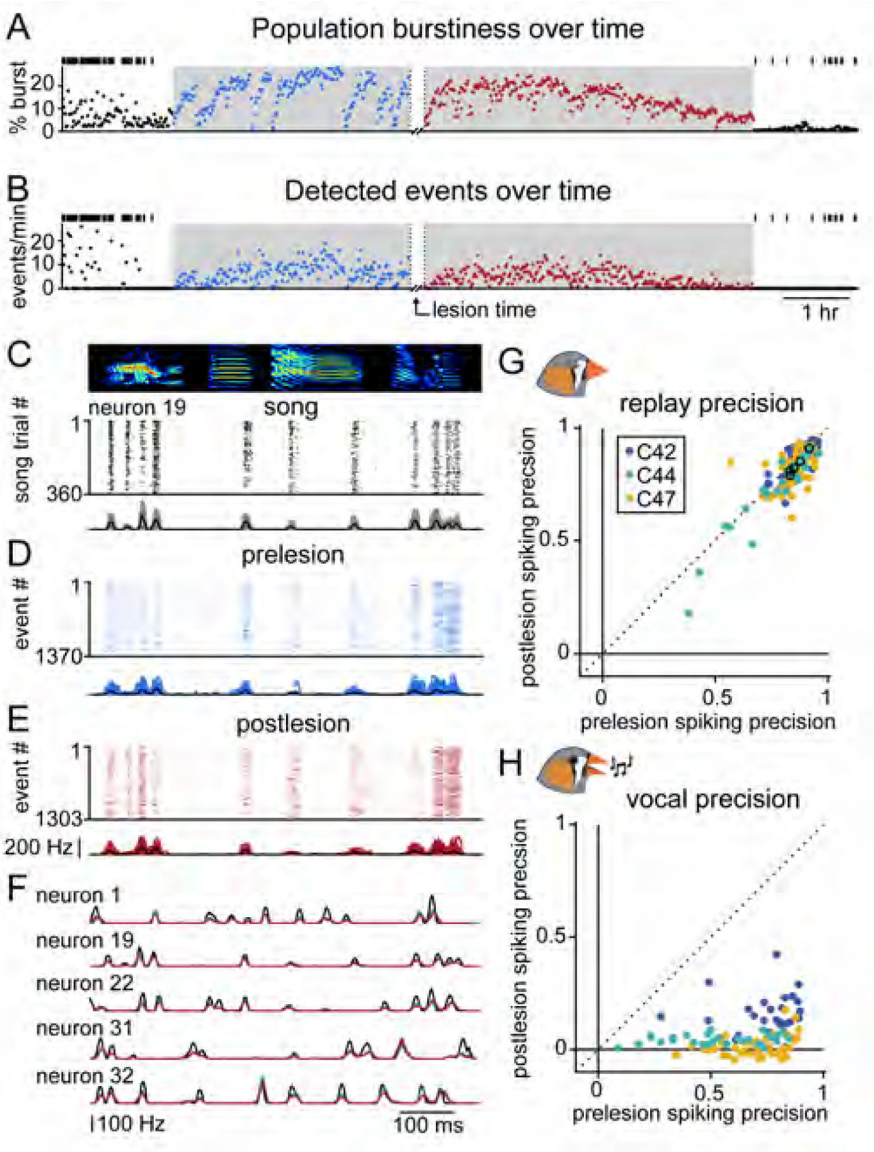

Figure 5. Sleep replay is unperturbed by thalamic lesion

(A and B) Percentage of spikes across the population that meet burst criteria (A) and the number of detected replay events (B) throughout the recording duration for Bird C44. Bin size = 1 min. Lights off indicated by shaded region; black vertical ticks show timing of vocal production.

(C-E) Template aligned spiking activity during song (C), prelesion sleep (D), and postlesion sleep (E) for example neuron 19. Below, instantaneous firing rates for each song or replay event with average in black.

(F) Average instantaneous firing rates for song (black) and sleep replay (prelesion: blue; postlesion: red) for five example neurons.

(G) Pearson correlation scores between song activity and average prelesion or postlesion replay before and after Uva lesion for all birds (n = 134 neurons across 3 birds, slope = 0.96, 95% CI = [0.85, 1.07]). Black circles indicate neurons from (F).

(H) Pearson correlation scores for RA firing activity during introductory notes for all birds before and after Uva lesion (n = 117 neurons across 3 birds, slope = 0.08, 95% CI = [0.001,0.15]). Neurons with fewer than two spikes on average per trial were excluded from this analysis.

See also Figure S5 and S6.

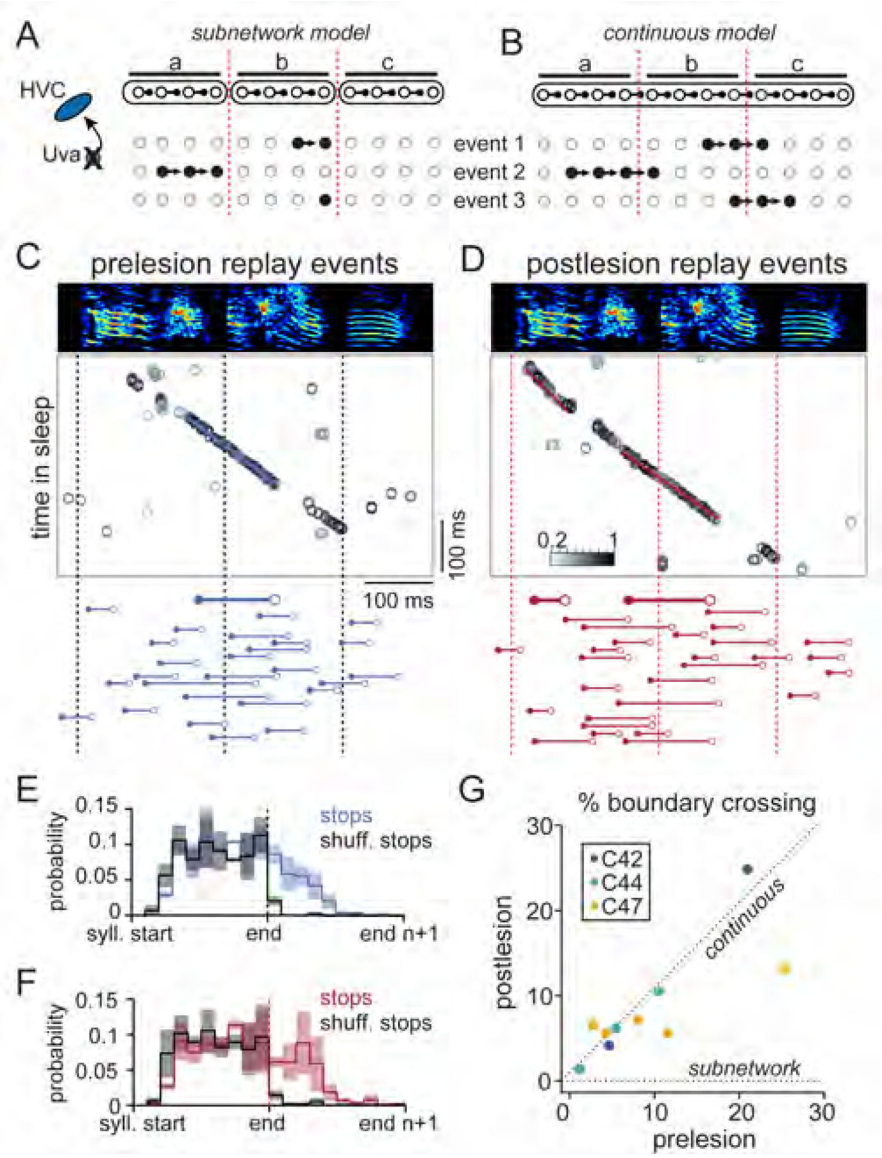

Figure 6. Sleep replay events cross syllable boundaries following Uva lesion

(A and B) Predictions for replay event structure following Uva lesion given the subnetwork model (A) or the continuous model (B).

(C and D) Example replay events before (C) and after (D) Uva lesion. (Top) Template matching assignments and corresponding detected events. (Bottom) The decoded song times for 20 example replay epochs (event start: filled circle, event stop: open circle, syllable boundaries: dashed lines). Examples illustrated above are bold.

(E and F) Pooled distribution of replay event stop times across 3 birds normalized to syllable boundaries before (n = 2,405 events) and after (n = 2,726 events) lesioning Uva. In black, a shuffled distribution (see Methods). Histograms show mean ± SEM.

(G) Percentage of detected sleep events that cross syllable boundaries from 3 birds. Each point represents a distinct syllable (n = 10). The incidence of syllable crossings does not

change following the lesion (Wilcoxon sign rank: $p = 0.70$), consistent with the prediction from the continuous model.

KEY RESOURCES TABLE

REAGENT or RESOURCE	SOURCE	IDENTIFIER
Antibodies		
Bacterial and virus strains		
Biological samples		
Chemicals, peptides, and recombinant proteins		
N-methyl-DL-aspartic acid (NMA, 4%)	AA Blocks	17833–53-3
Critical commercial assays		
Deposited data		
Experimental models: Cell lines		
Experimental models: Organisms/strains		
Zebra finch (Taeniopygia guttata)	Magnolia Bird Farm, Anaheim, CA	N/A
Oligonucleotides		
Recombinant DNA		
Software and algorithms		
MATLAB	MathWorks	https://www.mathworks.com/products/matlab.html
KiloSort spike sorting software	Pachitariu et al., 2016	https://github.com/cortex-lab/KiloSort
Sleep replay decoder (Template-matching tool)	This paper	https://github.com/LongLabGit/TemplateMatching.git DOI: 10.5281/zenodo.5500262
Other		
High-density silicon probe (with integrated headstage)	Diagnostic Biochips	128–5 integrated
Chronic microdrive	Neuronexus	dDrive-xL
Assisted Fiber-optic & Electric Rotary Joint	Doric Lenses	AHRJ-OE_FC_AD_12_HARW
Omnetics cable adaptor	Doric Lenses	ADAPTER_HO12
Acquisition board	Intan Technologies	RHD Recording Controller (512 channels)
Stimulus generator	A-M Systems	Model 2100
Omnidirectional microphone	Audio-Technica	AT803
Audio amplifier	Presonus	Studio Channel